Roundness error stacking in assembled spherical roller bearings and its impact on rotor subcritical vibration

Measurement 229 (2024) 114461

Contents lists available at ScienceDirect

Measurement

journal homepage: www.elsevier.com/locate/measurement

Roundness error stacking in assembled spherical roller bearings and its impact on rotor subcritical vibration☆

Lorenzo Giorio [a,b,*], Raine Viitala [a], Eugenio Brusa [b]

[a] Department of Mechanical Engineering, Aalto University, Sähkömiehentie 4, Espoo, 02150, Finland
[b] Department of Mechanical and Aerospace Engineering, Politecnico di Torino, C.so Duca degli Abruzzi 24, Torino, 10129, Italy

ARTICLE INFO

Keywords:
Bearing roundness
Roundness error stacking
Bearing thickness variation
Thickness variation profile
Harmonic components
Conically fitted bearing

ABSTRACT

In industrial processes, large rotors are commonly operated below the critical speed, where bearings can be an important source of subcritical vibration. This paper presents a complete study and analysis of the roundness error stacking in rotor-bearing systems. The investigation on how the roundness error of tapered shafts is transferred through the bearing inner ring to the raceways during the assembly process allows to evaluate the final roundness profile of the raceways as the sum of the shaft roundness profile plus the inner ring thickness variation. The method's validity is verified for relative orientations and mounting conditions between the components.

A test case is presented in which 3D conical grinding is applied to a shaft tapered bearing installation seats, reducing the roundness error of installed bearings when compared to previous research results. The relevance of the study was proven with rotordynamic measurements, which show that minimized roundness error reduces vibrations.

1. Introduction

Reduction of vibration in rotating machinery is a key factor in increasing the machine life and improving modern industry efficacy, which has led to a rise in research related to precise components for large rotor-bearing systems. Large scale rotor-bearing systems are commonly used in various industrial fields, such as for example in the field of power generation, maritime industry, steel manufacturing plants and paper production. Unscheduled maintenance stops due to bearings failure as well as vibrational excitation due to the bearings can considerably increase costs. Additionally, the renewable energy production section, such as wind turbines, is increasing its market share [1] and safety and reliability of operations are key topics in ensuring high availability of critical infrastructure and successful operation.

In absence of active vibration control during operation, the reduction of vibrations during rotating machine operations has led to an increased need for precision manufacturing and measuring technologies for large rotor components and complete rotor-bearing systems.

Bearings are key elements of any rotating machine since they enable the rotational motion of the supported shaft and bear the loads. The typical bearing structures in large rotating machinery include either hydrodynamic journal and roller element bearings. Especially in cases where compliance against lateral loads and bending is needed, a spherical roller element bearing might be preferred. Despite quality control operations during the bearing production, bearing components always contain slight imperfection such as thickness variation and roundness deviations of the parts.

Typically, roller element bearings can be installed on the rotor using three different methods, which depend on the geometrical properties of the shaft. On cylindrical shafts, the bearing can be installed by means of a shrink fit, or using a conical adapter sleeve between the bearing inner ring (IR) and the cylindrical shaft. A tapered section can also be manufactured on the shaft itself, allowing to install the bearing with a conical bore directly onto the rotor shaft. In large bearings, the IR is generally thin and quite more flexible than the rotor shaft on which it is assembled. This causes the IR to adapt to the roundness shape of the rotor, causing the roundness deviation of the individual bearing components to become less significant. In all mounting methodologies, the final roundness profile of the raceways of a mounted bearing IR will be affected by the following component manufacturing errors: the roundness profile of the shaft installation seat, the thickness variation of the adapter sleeve when present and the thickness variation of the bearing IR itself [2]. In previous researches [3,4] the error stacking that

☆ This research was funded by the 19ENG07 Met4Wind project, which has received funding from the EMPIR programme co-financed by the Participating States and from the European Union's Horizon 2020 research and innovation programme.

* Corresponding author at: Department of Mechanical and Aerospace Engineering, Politecnico di Torino, C.so Duca degli Abruzzi 24, Torino, 10129, Italy.
E-mail addresses: lorenzo.giorio@polito.it, lorenzo.giorio@aalto.fi (L. Giorio), raine.viitala@aalto.fi (R. Viitala), eugenio.brusa@polito.it (E. Brusa).

https://doi.org/10.1016/j.measurement.2024.114461
Received 28 November 2023; Received in revised form 5 March 2024; Accepted 6 March 2024
Available online 11 March 2024

leads to the final roundness profile of the bearing IR was speculated, but a complete study and analysis of the assembly and error stacking strategy is still missing.

Roller element bearings are a common source of harmonic excitation in the subcritical rotating regime [5,6], causing subcritical resonance peaks that occur below the first natural frequency of the rotor. Rotor balancing is widely studied in the literature [7–12], but its effect is mainly visible for vibrations occurring once per revolution, with a smaller magnification effect of the subcritical vibration peaks.

Low order harmonics in the roundness profile deviation of bearing IR excite the rotor in the subcritical speed range. In simple terms, the ovality of the bearing IR mounted onto the shaft causes excitation twice per revolution, the triangularity three-times per revolution and so on. Therefore, the roundness deviation of a mounted bearing IR is linked to the harmonic subcritical vibration of the supported rotor. The excitation caused by the bearing waviness was firstly investigated during the 1960s by Gustafsson and Tallian [13] and Yhland [14]. The experimental investigations showed that the number of lobes in the roundness profile (i.e., the harmonic or waviness components) of the bearing IR raceways is an important source of vibratory excitation when multiplied by the rotating frequency of the IR itself. This was also proposed later in [6] and confirmed by Aktürk [15] in his mathematical model that included bearing elements waviness. An upgraded model based on the latter was then used to study the excitation caused by a defected IR [16].

Liu et al. [17] measured the vibration of a ball bearing outer ring and compared that to the waviness of the inner and outer race of the bearing, finding that close to the natural frequency of the system the highest contribution to the vibration was given by the waviness. In [18,19] the authors proposed a multi-body modeling of a flexible rotor including elastic ball bearings, studying the effect of bearing IR waviness on the rotor dynamic response. The authors found out that the resonances in the sub-critical regime were caused by the waviness of the bearings IRs, also highlighting that the excitation appears to be weaker if the phase angles of the waviness profiles of the two bearings differ from each other. The dynamic numerical model of a spherical roller bearing able to simulate waviness of the roller paths and presented in [20,21] was used in [22–24] to investigate the subcritical vibration of large rotors, including both numerical and experimental results. The authors confirmed the importance of the waviness of the bearing IR roundness profile in the harmonic subcritical vibration response of the supported rotor.

To accurately predict the non-linear contact force for the sinusoidal waviness profile in bearing raceways, Liu et al. [25] developed a new rigid rotor system dynamic model with waviness in the support bearings, using the Johnson's extended Hertzian contact model. The proposed model is able to consider the variable curvature between sinusoidal surfaces in contact, while considering the lubrication condition, showing a difference up to 17.85% between Johnson's extended Hertzian contact model, Hertzian contact model and simplified Hertzian contact model.

In industrial applications, lubrication can greatly affect the service performances of ball bearings. In [26] the authors presented a new simulation model that combine rotordynamic and computational fluid dynamics to investigate the oil–air two-phase flow. The effects of the bearing rotation speed, cage clearance, and relative motion of ball on the lubrication characteristics are studied, showing that lubricating oil content in the bearing cavity decreases significantly with the increment of bearing speed. Additionally, it was observed that in the inner raceway the lubricating oil is disturbed by the opposite direction of movement, creating a higher content of lubricating oil on the side of the ball opposite to the bearing rotation. In the present paper, due to the relatively low rotational speed of big industrial shaft, the effect of lubrication will not be neglected.

Roundness measurement related researches are quite present in the literature, and studies related to the improvement of the accuracy and reduction of uncertainty, in addition to the comparison of roundness measurements, are available [27–32]. Unlike roundness measurements, thickness variation measurements and measurement methods of rings geometrical properties are seldom presented in the literature. The standard ISO 1132-1 [33] defines the thickness deviation as a single value, without discussion related to the actual complete profile, needed for its harmonic analysis. Some studies in the literature proposed devices and methods for measuring the thickness variation of bearing components [2,34,35].

The origin of the thickness variation in bearing elements was investigated, among others, by Deng et al. [36]. During the manufacturing process, the relatively thin bearing rings are deformed by the clamping forces. The turning and grinding operation performed, up to a round profile, on the bearing functional surfaces are carried out on a tensioned component, which at last lead to thickness variation profiles, dependent on the clamping method used by the machine tool.

In a recent research paper, Viitala et al. [3] published a study in which the roundness profile of mounted bearing IR was modified using steel strips between the rotor shaft and the conical adapter sleeve used for the assembly procedure. Of the five different geometries investigated, one was chosen to minimize the roundness error of the mounted bearing IR. The reduction of the roundness error contributed to decrease the vibration amplitudes in the whole subcritical response spectrum. In a later research, Viitala [4] presented a study in which compensative 3D grinding was used to minimize the roundness error of mounted bearing IRs. The grinding operation was performed on the cylindrical shaft underneath the conical adapter sleeve used for assembly, using the measurement of roundness of the mounted IR as feedback for the iterative manufacturing operations. The compensative 3D grinding reduced the roundness deviation in both bearing IRs of the rotor-bearing system, with a significant improvement in the rotor dynamic response in the subcritical regime, also when compared to the results of [3]. The authors questioned the reliability of the steel strips method in real industrial application, also considering that the correct installation of the steel strips required multiple trial and error to arrive at the correct positioning. Moreover, the compensative 3D grinding on the cylindrical shaft coupled with the use of a conical adapter sleeve leaves room for improvements in the residual roundness error of the installer bearing IRs, and presented some unwanted higher order subcritical resonance peaks.

In order to complete the investigation and analysis of the error stacking methodology that leads to the final roundness profile of installed bearing IR, the present paper reports the successful verification that the roundness profile of bearing IR raceways mounted on tapered shafts can be accurately evaluated though the error stacking method, i.e., the final roundness profile is equal to the sum of the shaft roundness profile plus the thickness variation of the bearing IR. A shaft stud with a tapered installation seat has been designed and manufactured to host a spherical roller element bearing IR. The effect of different relative orientations between the components and the effect of different mounting conditions has been deeply investigated, showing that exists an optimal orientation, dependent on the measuring axial location, between the shaft and bearing IR that minimizes the final roundness deviation, and that the results reported in the present paper hold true for various mounting conditions between the components. The experimental verification of the roundness error stacking was performed for several axial cross sections, multiple relative orientations between the assembled components and various mounting conditions matching real industrial applications, adding robustness to the methodology presented and providing an extended general significance to the assembled bearings roundness evaluation procedure presented. In order to maintain a single reference system between unmounted and mounted condition, and accurately evaluate the relative orientations between the assembled components, markings for the origin of the angular coordinate used for the roundness measurement should be

implemented, to overcome the challenge of correctly positioning the components during the assembly process.

The roundness error stacking methodology allows to more easily evaluate the final roundness profile of installed bearing IR, which is a difficult task to perform after assembly due to the large size of the system that do not allow the use of precision measurement equipment due to the size limitation.

In addition, the present paper extends the results of [4] by applying the 3D grinding methodology to tapered installation seats directly into the rotor shaft, to reduce the roundness error of the installed bearing IRs. Due to the large size of the shaft, conventional roundness measurement equipments could not be used, requiring the use of the four-point method [3,4]. The experimental measurements of the remaining roundness error after the compensative grinding showed a great reduction compared to the previous research. The rotor dynamic response measurements in the subcritical regime showed a significant reduction of the high order subcritical resonance peaks compared to the previously studied research in which the grinding operation was performed on the cylindrical shaft and adapter sleeves were used for the assembly of the bearings.

2. Methods

In this section, the key parameters of total roundness and thickness variation evaluation are described, together with the measurement methods used for the experimental campaign. The performed experiments to investigate the error stacking of the total roundness of the bearing IR are described in detail, with the additional description of the mounting method used to accurately mount the bearing onto the tapered seating. The procedures used to evaluate the effect of the relative orientation between shaft stud and IR as well as the effect of the mounting conditions are then presented.

2.1. Roundness and thickness measurements

Roundness is a property of a circle and is defined by the ISO standard 12181-1:2011 [37]. The roundness profile is an extracted circumferential line that can be obtained experimentally with a specific measuring instrument. From the profile, specific key parameters of roundness can be evaluated, such as the ones investigated in this paper, which are the RONt (peak-to-valley roundness deviation) and RONq (root-mean-square roundness deviation) [37]. The evaluation of both parameters depends on the choice of the center point of the roundness profile. Whitehouse [38] presented four methods to solve this problem, each one resulting in slightly different roundness parameters values. In this paper, the least square reference circle (LSCI) defined by the ISO standard was used for all the investigations.

If the harmonic content of the roundness profile or the form of the roundness error are required for the investigation, the measurement and analysis of the actual roundness profile is mandatory [28,29,31]. In this paper, in addition to the use of the roundness parameters above mentioned, the analysis of the results is carried out also considering the entire roundness profiles as well as their harmonic content in the frequency domain.

The thickness variation of bearing components is assessed by the ISO 1132:2000 [33,39], which defines it as a single value. The standard does not provide information on the measurement of the actual thickness variation profile, which is mandatory to discover the profile shape and the extraction of the harmonic components. In this paper, the thickness variation profile is evaluated with reference to Fig. 1 as the difference between the deviations of corresponding points in the angular coordinate of the external and internal profiles, as

$$T\left(\theta_i\right) = R_{ext}\left(\theta_i\right) - R_{int}\left(\theta_i\right) \tag{1}$$

where θ_i is the angular position, $R_{ext}\left(\theta_i\right)$ is the point deviation from the reference circle of the external profile at the specific angular position, $R_{int}\left(\theta_i\right)$ is the point deviation from the reference circle of the internal profile at the specific angular position and $T\left(\theta_i\right)$ is the thickness variation value at the specific angular position.

Harmonic analysis is often used in the analysis of roundness. The 1/rev frequency domain is selected so that the dynamic content of the profile is expressed as an amplitude and a phase for each Undulation Per Revolution (UPR) number [37]. In this way, the first harmonic corresponds to a small eccentric movement of the center point, the second to ovality, the third to triangularity and so on [40].

To represent the harmonic content of the profile in the frequency domain, the Fast Fourier Transformation is employed. Typically, when considering roundness measurements, only higher than the first order components (UPR ≥ 2) are relevant, as the zeroth and the first waviness components (offset and eccentricity, respectively) can be compensated by choosing the reference system origin in the center of the reference circle LSCI. This, however, does not hold for thickness variation, as its first order harmonic component cannot be compensated away with a coordinate system selection, but depends on the manufacturing error of the component between the internal and external profile center point. In rolling element bearing, such error is typically quite low and can be excluded from the investigation.

The selection of the frequency domain also allows for the application of Gaussian filtering of the harmonic content of the profiles. The attenuation function of the Longwave-pass filter is given in the ISO standard 12181-2:2011 [41], as a function of the cut-off frequency expressed in UPR. In this paper, all the roundness profiles analyzed are filtered with a 15 UPR Longwave-pass Gaussian filter, as in the rotordynamics point of view the harmonic components of interest are the first 5–8.

2.2. Four-point method and rotor dynamic measurement

In the test case presented in Section 4 the roundness profiles of the installed bearing were conducted using the four-point method [3,4,42,43] due to size and weight limitations of traditional roundness measurement equipment. The four-point method is a combination of the two-point diameter measurement method and the Ozono three-point method. This method is able to measure and separate the roundness profile and the center-point movement of a rotating workpiece. The run-out signals were acquired in the middle of both of the roller element raceways of the bearings from four Heidenhain MT 12 straight incremental length sensors, with Heidenhain IK220 interface electronics. 1024 samples per revolution were measured using a rotary encoder to ensure equal angular spacing between the samples. The experimental signals were later analyzed in MATLAB® to extract the roundness profiles and its harmonic components applying the four-point method. The rotor dynamic response in the subcritical regime was also measured using the four-point method: as the method is able to separate the roundness profile and the center-point movement of a rotating workpiece, it ensure an accurate acquisition of the center-point movement of the rotor, without being affected by the rotor roundness profile in the particular cross-section. The rotor displacement in the middle cross-section was measured using four laser triangulation sensors Matsushita NAIS LM 300, acquired by National Instruments USB-6215 data acquisition card. 1024 samples per revolution were measured using a rotary encoder to ensure equal angular spacing between the samples. The rotor response was measured in a rotating frequency range from 4 Hz to 18 Hz with 0.2 Hz increments, using 100 synchronously averaged revolutions for each rotating frequency. The four-point method was then applied to the low-filtered analog signals to obtain the center-point displacement and its harmonic components. To mitigate the effect of external factors in the experimental measurements of the rotor center-point movement, the tests were carried out in a temperature and ventilation controlled laboratory.

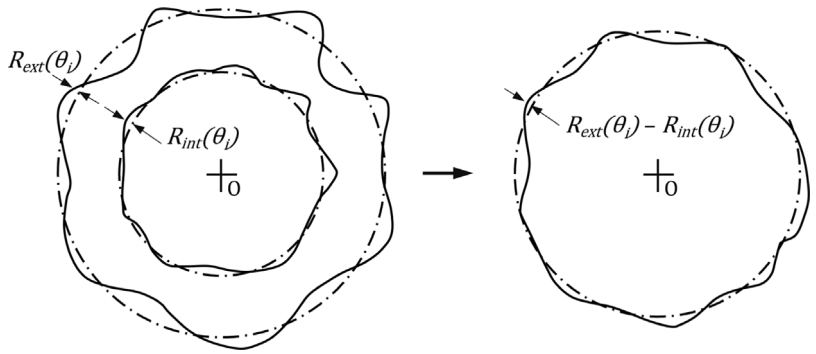

Fig. 1. Thickness variation calculation. O is the reference system origin and center of the reference circles, $R_{ext}(\theta_i)$ is the point deviation from the reference circle of the external profile and $R_{int}(\theta_i)$ is the point deviation from the reference circle of the internal profile, both measured at the specific angular position θ_i.

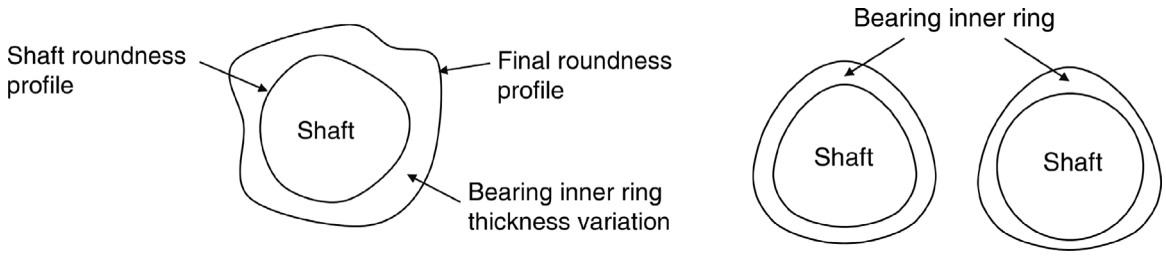

Fig. 2. Schematic representation of the final roundness profile of the IR due to the stacking of the shaft roundness error and the IR thickness variation (left). Schematic visualization of the roundness error formation of an installed bearing IR in two specific examples (right), modified from [2].

2.3. Stacked roundness error

In previous studies [3,4], the external roundness profile of a bearing IR has been assumed to consist of the shaft roundness error, thickness variation of the possible conical adapter sleeve as well as the thickness variation of the bearing IR itself. Thus, the clearance of an installed roller element bearing may be affected by the thickness variation leading to declined wear and dynamic behavior properties.

In the experimental measurements presented in this study, the conical IR of the bearing is installed directly onto a tapered shaft, therefore avoiding the presence of a conical adapter sleeve. The manufacturing error in each component is assumed to stack to the final roundness profile of the bearing IR outer profile, as presented in Fig. 2 on the left. In large bearings, the ring is relatively thin and flexible compared to the rotor shaft and housing in the final assembly. Thus, the rings deform to the shape of the adjacent parts and the roundness of individual components becomes less significant. In Fig. 2 on the right, a schematic visualization of the roundness error formation of an installed bearing IR is reported. In both depicted cases, the roundness error of the external surface of the bearing IR (in this case the 3rd harmonic component, triangularity) is the same, but in the former it is caused by the roundness error of the shaft, on which the relatively thin, but evenly thick IR has been tightened and thus deformed, while, in the latter, the roundness error is caused by the triangular thickness variation of the bearing IR mounted on a perfectly circular shaft. In real cases, the external roundness profile of the IR is a combination of both these error types.

For large bearings, in which the IR is relatively thin and flexible compared to the rotor shaft, the thickness variation of the IR can be assumed to remain constant between unmounted and mounted conditions, i.e. the displacement of the inner and outer profiles of the IR due to the assembly process is equal. In such case, the thickness variation of the IR can be measured in unmounted condition using the roundness profiles of the inner and outer surfaces of the IR, as explained in (1). For a specific axial location of the shaft-bearing assembly, indicating the angular coordinate with θ, the roundness profile of the IR raceway in mounted condition $R^*_{ext,IR}(\theta)$ is therefore assumed to be evaluated as:

$$R^*_{ext,IR}(\theta) = R_{Shaft}(\theta) + T_{IR}(\theta) \tag{2}$$

where $R_{Shaft}(\theta)$ is the roundness profile of the shaft in unmounted condition and $T_{IR}(\theta)$ is the thickness variation profile of the IR, assumed constant between unmounted and mounted conditions for large bearings. $T_{IR}(\theta)$ can be evaluated from (1) as the difference between the roundness profiles of the internal and external surfaces of the IR in unmounted condition, $R_{ext,IR}(\theta)$ and $R_{int,IR}(\theta)$ respectively:

$$T_{IR}(\theta) = R_{ext,IR}(\theta) - R_{int,IR}(\theta) \tag{3}$$

2.4. Pearson's correlation coefficient

In order to assess the similarities between two distinct roundness profiles, different methods have been presented in the literature [44–46]. In this paper, the Pearson's Correlation Coefficient (PCC) was used to evaluate the similarities between the evaluated summed roundness due to the stacked roundness error and the experimental measurements in mounted condition.

The PCC, also known as Pearson product-moment correlation coefficient, measures how two time-series co-vary over time (or, more in general, as a function of their variable), and it is widely employed to assess similarities between signals. In formula, the PCC between two signals $S_1(\theta)$ and $S_2(\theta)$ can be evaluated as:

$$\mathrm{PCC}(S_1, S_2) = \frac{\sum_{K=1}^{N}[S_1(\theta_k) - \bar{S}_1][S_2(\theta_k) - \bar{S}_2]}{\sqrt{\sum_{K=1}^{N}[S_1(\theta_k) - \bar{S}_1]^2}\sqrt{\sum_{K=1}^{N}[S_2(\theta_k) - \bar{S}_2]^2}} \tag{4}$$

where $S_1(\theta_k)$ and $S_2(\theta_k)$ are the values of the signals at variable $\theta = \theta_k$ and $\bar{S}_1$ and $\bar{S}_2$ are the mean values of each signal.

The PCC gives an indication of the strength of the linear relationship between the two signals, expressed as a value between −1 and 1. Generally, the correlation is considered strong if the PCC value is >0.8.

Fig. 3. Mitutoyo RA-2200DS used for the experimental measurements.

2.5. Experimental procedure

In the following section, the device and methods used for obtaining the roundness profiles of the component and the experimental procedure used for the investigation are presented.

To determine the roundness profile of a workpiece cross-section, roundness measurement instruments with precision spindles can be used, which provide accurate rotation for the part. An example of such instrument is the Mitutoyo RA-2200DS visible in Fig. 3 used in this research.

During the rotation of the part, roundness is measured with a single displacement probe after carefully carrying out the centering procedure provided by the instrument manufacturer to guarantee the correct positioning of the part on the precision spindle and avoid the limaçon error [6,47]. The signal of a single displacement probe will consist of the center-point motion of the cross section plus the run-out displacement of the profile. The former content of the signal is automatically excluded by a compensation performed in the measuring software before the extraction of the roundness profiles.

Following the technical specification of the instrument provided by the manufacturer, the radial rotational accuracy of the instrument can be evaluated as a function of the probing height H from the rotating plane as $(0.02+3.5H/10000)$ µm. For the research presented in this paper, all the measurements were performed for a probing height lower than $H < 150$ mm, resulting in an uncalibrated radial rotational accuracy lower than 0.0725 µm.

A shaft stud was designed and manufactured for the specific experimental investigation and a schematic representation is reported in Fig. 4.

The shaft stud is composed of a tapered mounting surface for the bearing with a 1:12 taper as per the bearing manufacturer specification. This surface was machined using an angular grinding machine to achieve a taper angle very close to the actual bearing used during the experiment, therefore achieving good contact between the mating

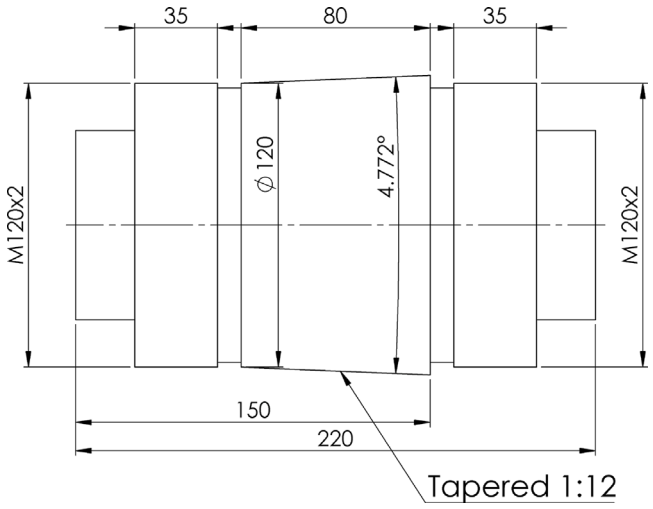

Fig. 4. Drawing of the shaft stud designed for the experimental campaign.

surfaces during the assembly. Two threaded sections M120 × 2 were manufactured on each side of the tapered section to accommodate the hydraulic nut used for the mounting and unmounting procedures explained in the following.

The IR used in the investigation comes from a double row spherical roller bearing (SRB) SKF 23124 CCK/W33 with a bore diameter of 120 mm.

The mounting procedure used for the assembly process of the bearing IR onto the shaft is the SKF Drive-Up Method [48], which incorporates the use of a hydraulic nut fitted with a dial indicator and a pressure gauge mounted on a pump. The correct fit of the bearing onto the tapered mounting region is achieved by controlling the axial displacement of the bearing from a starting position determined by a specific pressure applied to the hydraulic nut. The drive-up axial displacement applied to the bearing is accurately monitored by the dial indicator. Starting position pressure and axial displacement can be obtained by the manufacturer as a function of the shaft material and design, number of previous mounts and clearance reduction. A stage of the mounting procedure is depicted in Fig. 5(a).

The experimental procedure was carried out in two distinct steps, firstly related to the components in unmounted condition, and later for the mounted assembly (mounted condition).

In the initial unmounted condition, the following profiles were measured, with reference to Figs. 5(b) and 5(c):

- For the tapered section of the shaft stud, 80 profiles in the axial direction were measured at an uniform axial distance (location A of Fig. 5(c)).
- For the internal mating surface of the IR, 80 profiles in the axial direction were measured at an uniform axial distance (location B of Fig. 5(c)).
- For the external surface of the IR, 40 profiles were measured for each of the raceways (locations C of Fig. 5(c)).

The evaluation of the thickness variation of the IR was carried out from the last two sets of measurements. Particularly, for each of the external raceway measuring locations in unmounted condition, the two closest profiles at the same axial coordinate of the IR internal mating surface were interpolated to obtain the internal roundness profile and evaluate the thickness variation using (1). The thickness variation of the IR evaluated in unmounted condition and the shaft roundness profile at the same axial coordinate are used to numerically evaluate the summed roundness of the raceway in mounted condition.

The experimental measurements of the roundness profiles of the IR raceways in mounted condition were carried out for 4 different angular

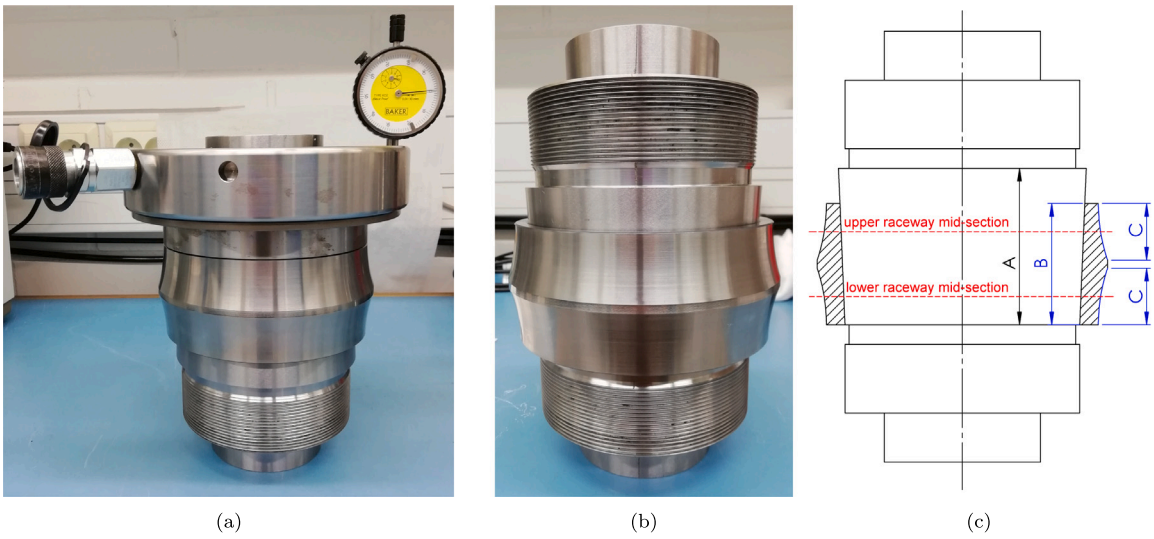

Fig. 5. (a) Installation of the IR on the shaft stud using the SKF Drive-Up Method with hydraulic nut. (b) Assembly of the shaft stud and IR in mounted condition. (c) Assembly scheme with indication of the experimental measurement locations; location A is the tapered section of the shaft stud, location B is the IR internal mating surface and locations C are the IR upper and lower raceways.

orientations between the components and for 2 different mounting conditions explained thoroughly in 2.5.2, which corresponds to 2 different reductions of internal clearance of the bearing. A single reference marking was created on the shaft stud to identify the starting angular position, while markings at 10 degrees intervals were created on the bearing IR. The careful alignment of the shaft marking with the IR marking allowed to realize the relative angular orientations used in the study. For each of the 8 measuring setups in mounted condition the following experimental procedure was employed:

1. The bearing IR was aligned to the shaft stud, using the angular marking corresponding to the orientation under study and the shaft marking.
2. The bearing IR was assembled using SKF Drive-Up Method through the use of the hydraulic nut. The axial displacement was selected to obtain the clearance reduction under investigation.
3. 40 roundness profiles were measured for each of the raceways.
4. The bearing IR was disassembled using the hydraulic nut.

2.5.1. *Effect of orientation*

To quantify the effects that the orientation of the bearing IR on a turned shaft has on the roundness parameters, the bearing IR was installed on the shaft stud and the roundness profiles of the bearing raceways were measured with the Mitutoyo RA-2200DS. The bearing IR was then removed and rotated by 90 degrees, and the measurement repeated. This operation was performed 4 times, to obtain roundness profiles corresponding to angular relative orientation equal to $0 - 90 - 180 - 270$ degrees between IR and shaft stud. The rotational angular increments were performed by aligning the corresponding marking of the IR with the singular marking on the shaft stud (located at the 0° of the angular coordinate θ). The example of angular orientation $\Delta\alpha = 90°$ is visible in Fig. 6, where the reference system drawn is referred to the working coordinate of the measuring instrument.

In Fig. 7 the effect of the relative orientation of the components on the mating surfaces between shaft and IR is reported. In particular, the blue line represents the roundness profile of the shaft tapered surface R_{shaft} (at the upper raceway mid-surface location) and the dashed red line represents the thickness variation profile of the IR, T_{IR}, measured experimentally in the global reference system at the same axis location (which corresponds to the nominal mounting condition with $\Delta\alpha = 0°$). The application of a relative orientation equal to $\Delta\alpha = 90°$ between the two components, with reference to Fig. 6, circularly shifts the thickness variation profile to the new location (solid red line). The rotation of the profile can be obtained without a new experimental measurement by applying a circular shift of the correct angle $\Delta\alpha$ to the measured data vector in the global reference system. The thickness variation profile evaluated at the correct relative orientation can then be used for stacking the error in the calculation process and evaluate the new summed roundness of the IR raceway.

2.5.2. *Effect of mounting condition*

To quantify the effects that the mounting condition of the bearing IR on a turned shaft has on the roundness, 2 different mounting conditions based on the SKF Drive-Up Method were employed in the experimental campaign. In particular, it was opted to use mounting conditions that result in a reduction of the internal clearance of:

- $\Delta r = 0.45‰$ of bore diameter d, which is generally employed for common applications.
- $\Delta r = 0.50‰$ of bore diameter d, advised for heavy loads applications, such as installations on paper machines.

The choice of the two mounting conditions represent the two extreme condition for radial internal clearance reduction in typical industrial application, following the specifications dictated by the manufacturer's manual [49] and the Drive-Up Method calculations [48]: values lower than $\Delta r = 0.45‰$ do not prevent the inner ring from loosening, while values greater than $\Delta r = 0.5‰$ (equivalent, in the case of the bearing in question, to a reduction in radial internal clearance equal to $\Delta r = 0.06$ mm) lead to a reduction in the fatigue life of the bearing. In specific cases where higher mounting pressure is required, special bearings with hardened inner rings should be used to avoid the risk of fractured inner rings.

Considering the experimental case with 6 or more previous mounts of the bearing onto the shaft stud, the SKF Drive-Up Method calculation for the particular assembly under study resulted in an initial pressure of 1.77 MPa applied to the hydraulic nut SKF HMV 24 E for both clearance reduction, and an axial drive-up displacement of 0.64 mm for the former mounting condition and 0.73 mm for the latter one.

3. Results and discussion

The results from the shaft stud tapered section measurements, bearing IR thickness variation measurements and bearing raceways evaluated summed roundness profiles and experimental measurements are

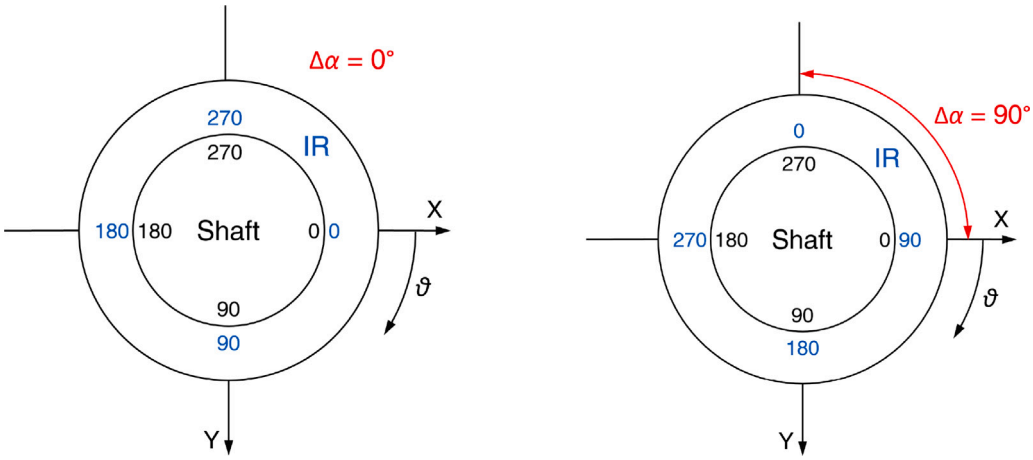

Fig. 6. Assembly process of shaft and IR including a relative orientation $\Delta\alpha$ between the components. X and Y are the global reference system axes and θ is the angular coordinate.

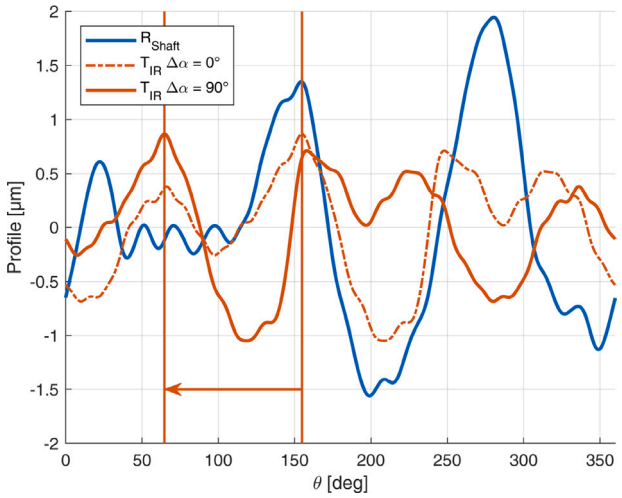

Fig. 7. Effect of the relative orientation $\Delta\alpha$ during the stacking process of the error. The blue line is the roundness profile of the shaft tapered surface R_{shaft}. The dashed red line is the experimentally measured thickness variation profile of the IR, T_{IR}, which corresponds to the nominal mounting condition with $\Delta\alpha = 0°$. The solid red line is the T_{IR} profile circularly shifted to the left by $\Delta\alpha = 90°$, used to evaluate the IR raceway summed roundness in the corresponding mounting condition.

presented and analyzed in the angular domain both in polar and expanded profiles, and as harmonic component distributions in the frequency domain. The validation of the error stacking process in estimating the final raceway roundness is performed by evaluating and comparing roundness parameters RONt and RONq, and evaluating the PCC between summed and experimentally measured profile, for all relative angular orientations between the components and mounting conditions investigated.

It was observed that the axial measurement location presented a negligible difference in the results of both unmounted and mounted conditions and thus the analysis will focus on two specifically selected locations. In particular, the results and discussion will be presented for the upper and lower raceway mid-sections, both indicated as red dashed lines in Fig. 5(c).

Considering the components singularly in unmounted condition, the first observation can be done on the roundness profiles of the shaft and the thickness variation of the bearing IR at the axial coordinates corresponding to the upper and lower raceway mid-sections. The axial coordinates chosen to locate the two measuring locations correspond to the mounting condition with $\Delta r = 0.50‰ \times d$, where d is the bore diameter of the bearing.

In Fig. 8 the polar plots of the roundness profiles on the shaft tapered section at the upper (left) and lower (right) raceway mid-sections are shown. The profiles present low values of total roundness RONt < 4 μm due to the manufacturing process that included the use of an angular grinding machine as previously explained. In both locations, the overall shape of the profiles presents a triangular component, which will be better shown in the frequency domain (Fig. 9). The variation due to the different axial locations between the two profiles is negligible, and can be again explained by the manufacturing process of the tapered section of the shaft stud.

In Fig. 9 the harmonic content of the shaft roundness profiles is depicted in the 1/rev domain. The first 15 harmonics (UPRs) are depicted, as the profiles represented in the polar and developed plots have been filtered with a Gaussian filter with cut-off frequency at 15 UPR as explained in the Methods section; the harmonics amplitudes in the frequency domain are not filtered, though, and represent the total harmonic content of the experimentally measured profiles without filtering. The majority of the harmonic content is contained in the third (triangularity) and second (ovality) harmonics, with contained differences of the amplitude between the two measuring locations. Negligible differences for the first eight harmonics can also be observed in the phase diagrams, confirming the similar shape of the roundness profiles. Above the 8th harmonic, the amplitudes are so small that the phase differences are acceptable.

The negligible variation in the amplitude and harmonic content of roundness profiles was also observed for all the other 80 measuring locations investigated on the tapered section of the shaft.

The polar plots of Fig. 10 describe the thickness variation of the bearing IR, at the upper (left) and lower (right) raceway mid-sections. The thickness variation is minimal with a total value <2 μm. As explained in the Methods section, the IR thickness variation was evaluated as the difference between the roundness profiles of the raceway and the internal tapered surface of the ring at the same axial location. The major contribution to the thickness variation depicted in the figure is due to the internal mating surface of the IR, as the roundness of the raceway is very low due to the accuracy of the manufacturing process of the surface.

In Fig. 11 the harmonic content of the IR thickness variations at the two measuring locations is reported. In both cases, the harmonic content is mainly contained in the first 4 harmonics, with differences in their phases.

To show the close agreement of the roundness profiles evaluated with the stacking process of the shaft roundness and IR thickness variation in evaluating the final external roundness of the IR raceway, compared to the experimental measurements, one case is reported in the following in detail. In particular, Figs. 12–14 refer to the assembly at relative orientation $\Delta\alpha = 0°$ and mounting condition $\Delta r = 0.50‰ \times d$.

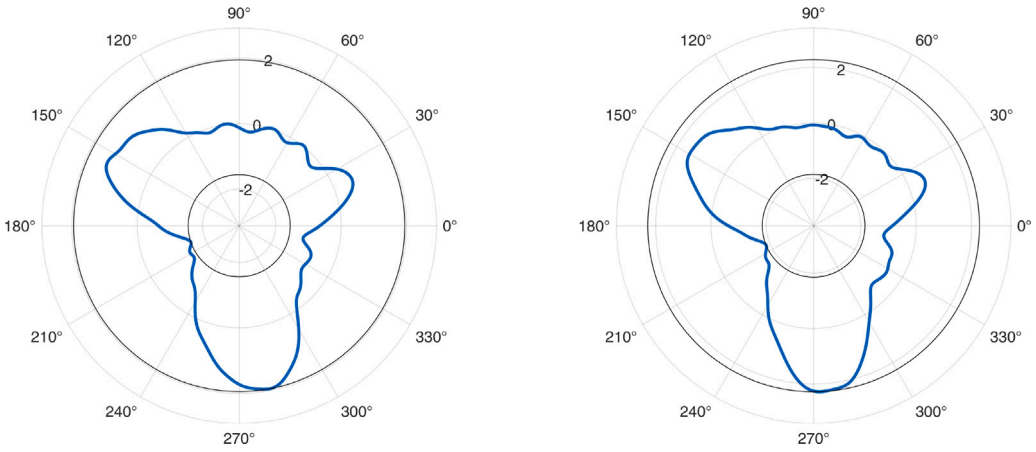

Fig. 8. Roundness profiles of the shaft tapered surface, for the upper (left) and lower (right) raceway mid-sections measuring locations. The radial axis unit of measurement is μm.

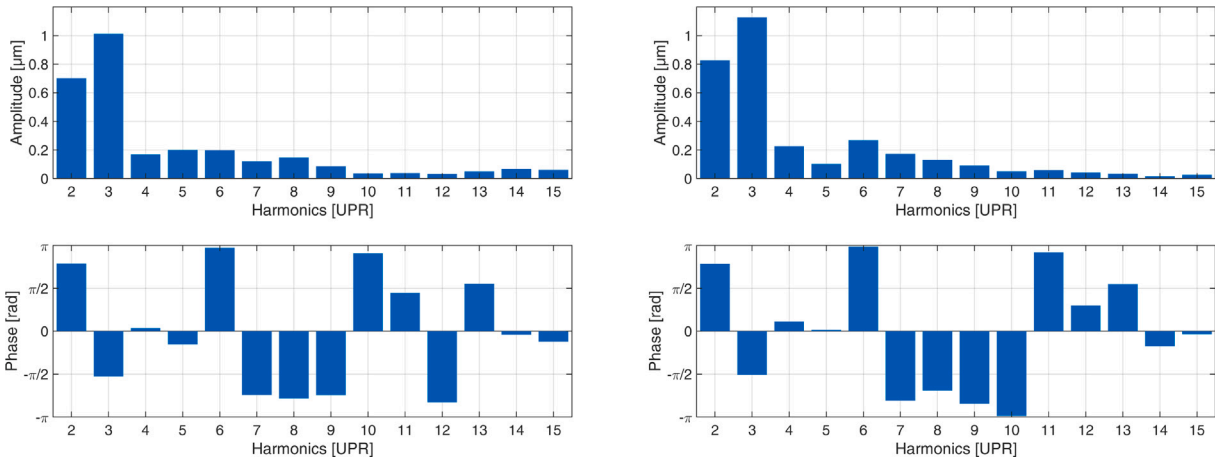

Fig. 9. Harmonic content of the roundness profiles of the shaft tapered surface, for the upper (left) and lower (right) raceway mid-sections measuring locations.

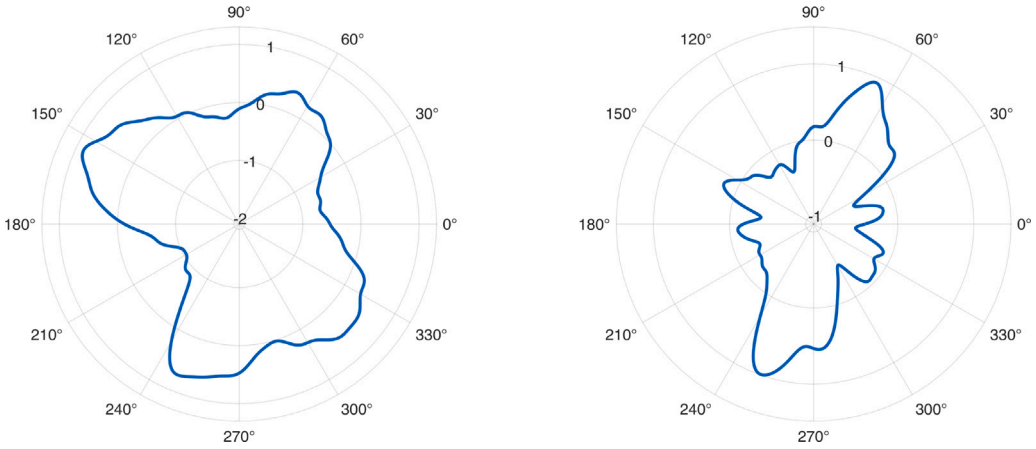

Fig. 10. Thickness variation profiles of the bearing IR, for the upper (left) and lower (right) raceway mid-sections measuring locations. The radial axis unit of measurement is μm.

The comparison of the summed and experimentally measured roundness profile of the IR raceways in upper (left) and lower (right) mid-sections are reported in Fig. 12 in polar coordinates and in Fig. 13 as a function of the angular coordinate θ. The very good agreement between the evaluated profile with the stacking summation process (in red) and the experimental one (in blue) is observed, along the whole circular profile. In Fig. 13, the black dashed line represents the roundness profile of the IR raceway in unmounted condition, i.e., before the assembly process. As it can be seen, the characteristics of the mounted profiles differ notably from the black line, confirming that the final profile of the bearing raceways in mounted condition is due to the sum of the shaft roundness plus the IR thickness variation, and not to a pre-existent deviation of the raceway itself.

The harmonic content comparison of the profiles is reported in Fig. 14 for both measuring locations. Considering the amplitude of the harmonics, close agreement between the evaluated and experimental

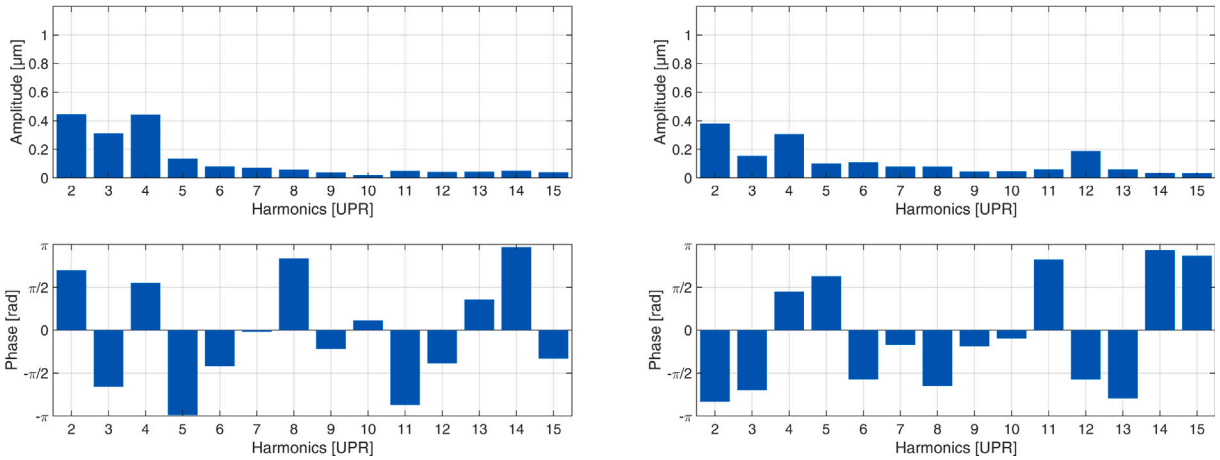

Fig. 11. Harmonic content of the thickness variation profiles of the bearing IR, for the upper (left) and lower (right) raceway mid-sections measuring locations.

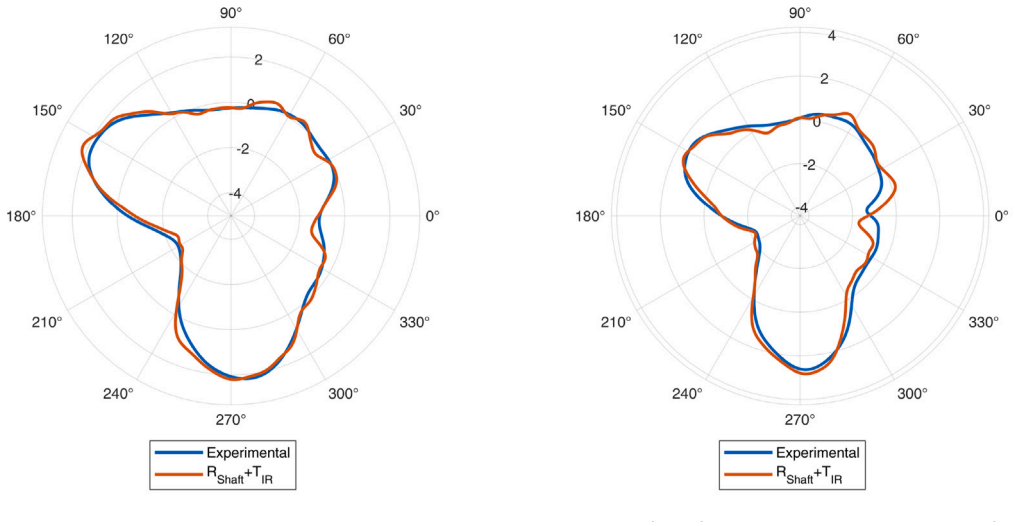

Fig. 12. Comparison between experimentally measured roundness (blue) and summed roundness (red), for the upper raceway mid-section (left) and lower raceway mid-section (right) measuring locations, in mounted condition. The radial axis unit of measurement is µm.

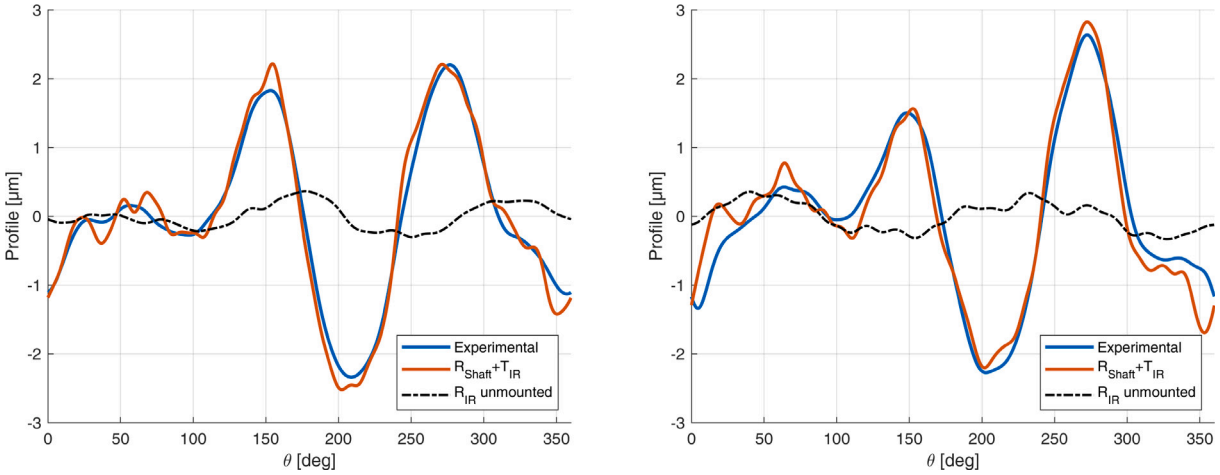

Fig. 13. Comparison between experimentally measured roundness (blue) and summed roundness (red), for the upper raceway mid-section (left) and lower raceway mid-section (right) measuring locations, in mounted condition. The dashed black line represents the experimentally measured external roundness profile of the IR raceway mid-section R_{IR} in the corresponding measuring location, in unmounted condition.

profiles is visible for all the harmonics in both locations, while for the phase diagram a more detailed explanation is reported in the following.

Focusing on the phase diagram in the left side of Fig. 14, relative to the upper raceway mid-section, close agreement of the phase values can

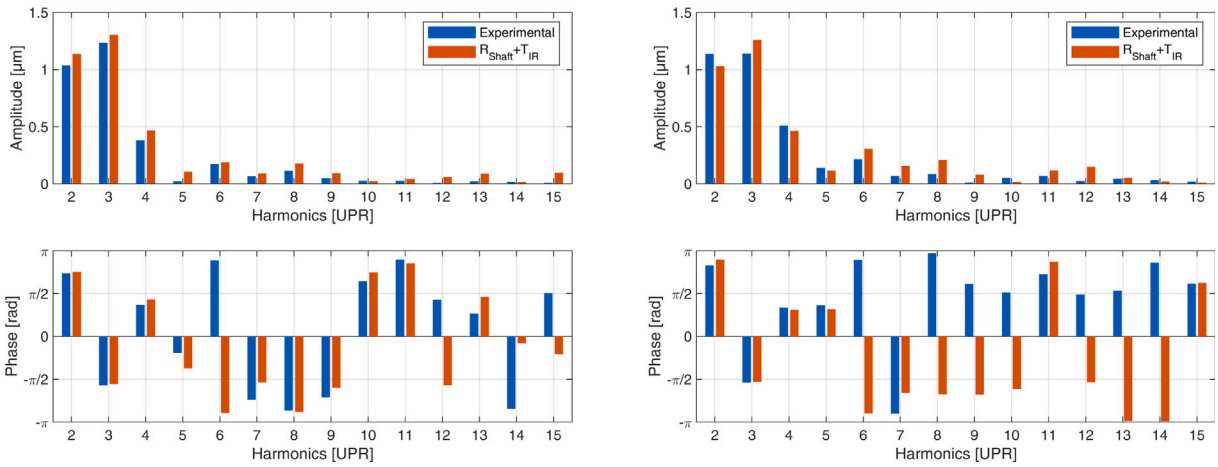

Fig. 14. Harmonic content comparison between experimentally measured roundness (blue) and summed roundness (red), for the upper raceway mid-section (left) and lower raceway mid-section (right) measuring locations.

be noted for all the harmonics up to the 11th: the difference visible for the 6th harmonic is due only to the choice of the plotting domain of the phase diagram itself, that here is represented in $[-\pi;\pi]$. Due to the periodicity of the phase, a different choice of the plotting domain, for example $[0;2\pi]$, will remove this difference, as the red bar with a value a little lower than $-\pi$ will be converted in a value slightly bigger than π. Looking at the phase diagram in the right side of Fig. 14, relative to the lower raceway mid-section, agreement of the harmonics phases between the summed (red) and experimental (blue) profiles can be observed up to the 8th harmonic. Higher harmonics present bigger differences in the phase, but their contribution to the total content of the profile is very low, as visible from the amplitude of these harmonics.

3.1. Effect of orientation

To analyze the effect of the relative orientation between shaft stud and IR during the assembly process, the stacked error evaluated through the summation of the shaft roundness and IR thickness variation has been calculated for $\Delta\alpha$ increments of 10°. The peak-to-valley roundness deviation RONt and the root-mean-square roundness deviation RONq of the summed profiles obtained are reported in Fig. 15 as the red lines for the upper (left) and lower (right) raceway mid-sections, considering the mounting condition with $\Delta r = 0.50‰ \times d$ of clearance reduction.

The relative orientation $\Delta\alpha$ between the two components has a strong impact on the total roundness of the raceway profile, with a variation over 50% for the upper raceway mid-section and around 40% for the lower raceway mid-section. It can also be observed that exists an optimal orientation between the components that minimize the total roundness of the profile, but the actual value of $\Delta\alpha$ that assures such condition depends on the axial location of the measurement. In particular, a value of $\Delta\alpha = 300°$ minimizes the RONt of the upper measuring location, while a $\Delta\alpha = 50°$ is necessary to minimize the RONt of the lower one. It should be also noted that the minimum possible value of RONq for the lower raceway mid-section is expected at a relative orientation of $\Delta\alpha = 60°$ between the two components. Therefore, in the assembly process, the optimal orientation between the two components not only depends on the axial position chosen for the evaluation, but also on the roundness parameter used. A comprehensive optimization problem should take into consideration also the latter.

The blue dots in Fig. 15 report the experimental measurement in the same mounting conditions for the four investigated orientations of $0 - 90 - 180 - 270$ degrees between IR and shaft stud. The experimental measurements follow the same trend as a function of the relative orientation, with a maximum absolute distance between summed and experimental measurement RONt equal to $0.69\,\mu m$ on the upper raceway mid-section and $0.63\,\mu m$ on the lower one. For the RONq parameter, the maximum distance recorded between summed and experimental measurement is $0.10\,\mu m$ at $\Delta\alpha = 0°$ for the upper raceway mid-section, and $0.11\,\mu m$ at $\Delta\alpha = 270°$ for the lower raceway mid-section measuring location. These differences may seem notable, but it should be highlighted that the case under study presents a precise machining operation through grinding in the shaft stud manufacturing process, resulting in very contained total roundness of the final assembly (the maximum RONt expected in the worst angular orientation of the components is $4.9\,\mu m$, evaluated though the stacked roundness process for $\Delta\alpha = 350°$ on the upper raceway mid-section). In cases where the roundness of the shaft is greater, the absolute difference between the summed and experimental roundness is expected to change insignificantly, while the RONt of the raceway would increase, reducing the percentual weight of the error.

Table 1
Pearson's Correlation Coefficient evaluated between the summed and experimental roundness profile of the IR raceway, for the 2 measuring locations.

$\Delta\alpha$ [deg]	Upper raceway mid-section	Lower raceway mid-section
0	0.991	0.969
90	0.978	0.979
180	0.985	0.980
270	0.985	0.990

The roundness parameters shown in Fig. 15 condense the information contained in the complete roundness profiles into a single value. To have a better understanding of how well the error stacking process, which evaluates the final raceway roundness as the sum of the shaft roundness plus the IR thickness variation, estimates the experimentally measured raceway roundness, the Pearson's Correlation Coefficient (PCC) between summed and experimental roundness profiles can be evaluated. The visual comparison of the summed and experimentally measured profiles, for all 4 angular relative orientation investigated and both measuring location of upper and lower raceway mid-sections, is visible in Fig. 16; the corresponding PCC values are reported in Table 1.

The lowest recorded value of PCC of 0.969 is reported for $\Delta\alpha = 0°$ on the lower raceway, highlighting a very strong correlation between the summed and experimental profiles along the whole circumferential direction.

3.2. Effect of mounting condition

The effect of the 2 mounting conditions investigated on the roundness parameters RONt and RONq for the experimental and stacked roundness profiles of the raceways is visible in Fig. 17. As explained in

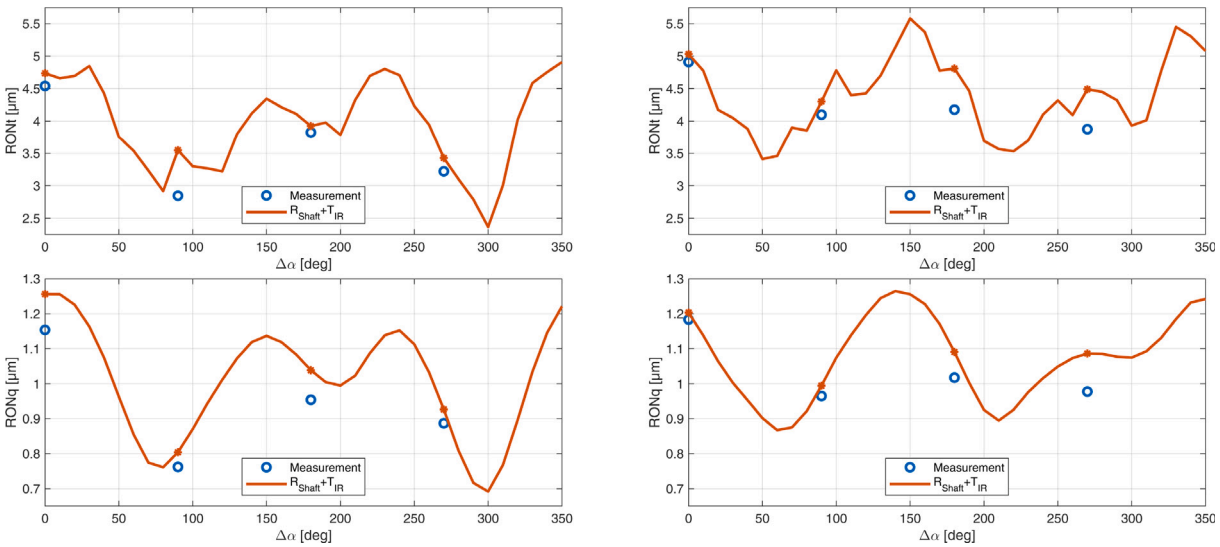

Fig. 15. Variation of the summed roundness RONt and RONq (red) as a function of the relative orientation $\Delta\alpha$ of the components, for the upper raceway mid-section (left) and lower raceway mid-section (right) measuring locations. In blue, the RONt and RONq of the experimentally measured profiles are depicted.

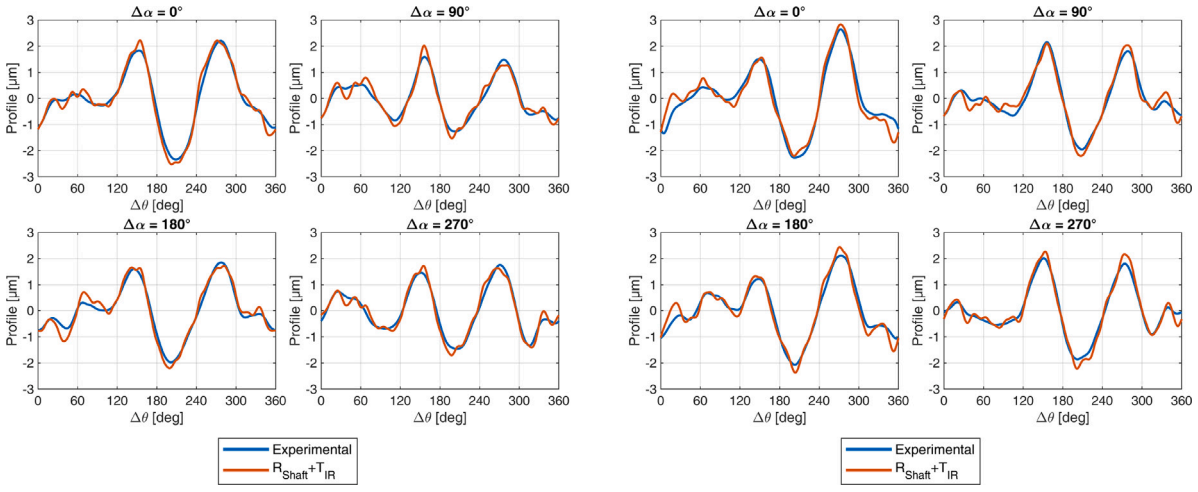

Fig. 16. Comparison between experimentally measured roundness (blue) and summed roundness (red) profiles as a function of the relative orientation $\Delta\alpha$ between the components, for the upper raceway mid-section (left) and lower raceway mid-section (right) measuring locations.

the Methods section, the difference between the 2 mounting conditions is a difference axial drive-up distance, which differs between the two cases by 70 µm. The manufactured shaft presents, as explained before, negligible differences in the roundness profiles along the axial direction. Concurrently, the bearing IR presents a smaller thickness variation in absolute value compared to the shaft roundness, and the axial position influence on the thickness variation is contained. Therefore, the effect of the mounting conditions on the roundness parameters is expected to be negligible, and this can be observed in Fig. 17. The variation of roundness parameters due to the different mounting conditions (represented by the blue/red color for $\Delta r = 0.45‰ \times d$ mounting condition, and by the light-blue/orange for the $\Delta r = 0.50‰ \times d$ mounting condition, where d is the bore diameter of the IR) is small compared to the effect of the angular relative orientation between the components. The methods reported in this paper to evaluate the final roundness profile though the stacking process of the errors and the sum of the shaft roundness profile plus the IR thickness variation is valid for both mounting conditions, taking into account the different axial drive-up distance during the selection process of the profiles of shaft roundness and IR thickness variation to be summed.

4. Test case: conical fit in paper machine

In order to complete and extend previous researches published in [3,4] that focused on the reduction of the subcritical resonance amplitudes of a paper machine roll by reducing the roundness error of the installed bearing IR, a new experiment was performed. In particular, unlike the previous mentioned researches that included the installation of the bearing IR onto a conical shaft using a tapered sleeve adapter, in the experiment presented in this paper the installation of the bearings IR was done directly onto tapered mounting surfaces, machined directly onto the shaft.

The roundness measurements and the rotor response measurements in this paper were conducted using the four-point method [3,4,42,43]. The main advantage of this method, in particular for large workpieces that cannot be measured with traditional roundness measurement instruments (such as the Mitutoyo RA-2200DS), is that it is able to separate the roundness profile from the rotor central axis movement reliably. Moreover, the use of the four-point method guarantees that the possible deformation of the roll could not affect the response measurements.

The rotor investigated in the present study was a paper machine roll already presented in previous research [3,4]. The rotor is supported on

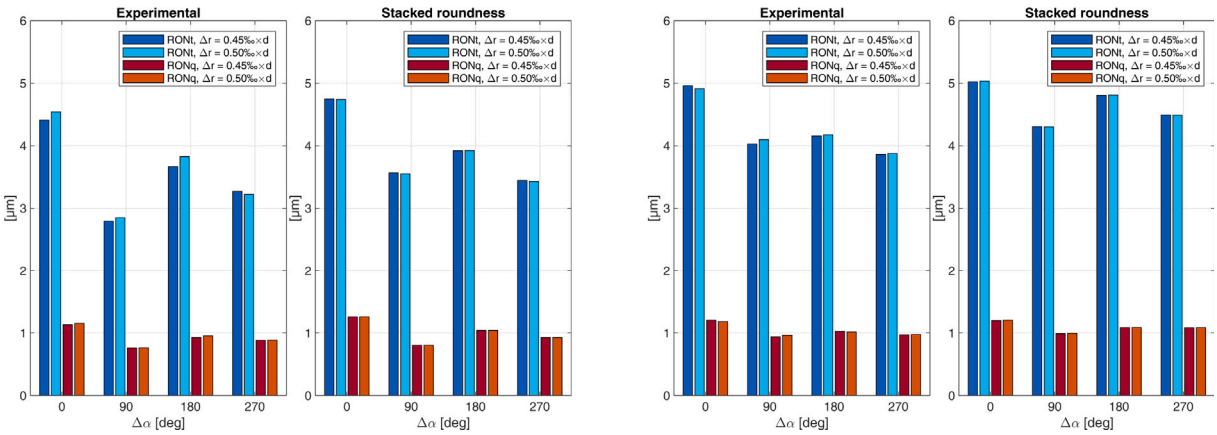

Fig. 17. Variation of the summed roundness RONt and RONq of the experimentally measured profile and the summed profile, as a function of the relative orientation $\Delta\alpha$, for 2 mounting conditions (in blue/red and light-blue/orange). The results are shown for the upper raceway mid-section (left) and lower raceway mid-section (right) measuring locations. Δr is the bearing radial internal clearance reduction in mounted condition and d is the bearing bore diameter.

each end by spherical roller element bearings SKF 23124 CCK/W33, the same model used for the experimental investigation reported in the previous sections of this paper. The installation of the bearings onto the shaft was performed using the SKF Drive-Up Method, with the use of the hydraulic nut.

The bearing IR roundness profiles were measured while installed on the rotor shaft, as visible in Fig. 18(a), to obtain the stacked roundness profile as it is during the rotor operation. In particular, the roundness profiles were measured in the middle of each raceway (upper and lower raceway mid-sections), for both the supporting bearings (tending end and drive end). The effect of the compensation grinding on the rotor response was investigated by measuring the response with the four-point method in the mid cross-section of the rotor using a measurement setup built on a computer numerically controlled rotor grinding machine, as visible in Fig. 18(b).

The tapered sections of the rotor used for the bearing installation were compensatively ground, as visible in Fig. 18(c), using the 3D grinding method developed by [50] for paper machine rolls. The final geometry of the installation seats is achieved with an iterative process using the roundness measurement data as feedback. Consequently, the tapered sections of the shaft were ground to a non-circular roundness profile, in order to minimize the roundness error of the installed bearing IR.

The experimental procedures used to measure the bearing IR raceway roundness profiles and rotor dynamic response are the same used in [4].

The results from the bearing IR roundness profile measurements after the compensative conical grinding are presented and analyzed in polar coordinates. The rotor response in the middle cross-section is presented in horizontal (X coordinate) and vertical (Y coordinate) directions as frequency domain spectra. The results of the present study are compared to the original geometry data and the data obtained after the roundness error minimization with compensative grinding of the cylindrical installation seat with a tapered adapter sleeve, both published earlier in [4]. The results coming from the previous publication [4] and used to compare the newly obtained roundness and rotor response data after the compensative conical grinding, are highlighted by citation in the following Figures captions.

4.1. Roundness measurement: results and discussion

Fig. 19 reports the bearings IR roundness profiles for the tending and drive end. The two roundness profile curves in red and blue represent the roundness profile measurements in the raceway mid-sections of both the roller element paths of the two row spherical roller element bearing.

The additional noise in the roundness profile curves, particularly in the drive side, that can be observed for the case of cylindrical installation seats, was completely eliminated in current case with conical ones. The compensative grinding of the conical bearing installations sites both in the drive and tending end of the rotor appears to be an additional improvement compared to cylindrical case. The roundness error of the bearing IR has been further reduced from 6.5 μm to 5.0 μm in the tending end and from 7.3 μm to 3.2 μm in the drive end. In relative terms, the reduction in the drive end was significantly greater.

The results clearly suggest that the use of a conical installation on the shaft, without the need of an adapter sleeve, can efficiently reduce the roundness error of the bearing IR when paired with the compensative grinding. Moreover, the downside of increased waviness that was observed in [4] for the case of cylindrical shaft and adapter sleeve is not present in this case, confirming the high usability of the method. The reduction of the roundness error in the drive side was substantially larger, but the final roundness error on both ends appears in the same range (5.0 μm in the tending end, 3.2 μm in the drive end).

4.2. Response measurement: results and discussion

The dynamic response of the rotor was measured in the mid cross-section for rotating speed in the range [4 Hz; 18 Hz] with 0.2 Hz increments. The chosen measurement discretization may capture the amplitudes and frequencies of the subcritical resonance peaks not as accurately as possible. However, the purpose of the present study is to investigate the change in the dynamic response caused by the compensative grinding, and not to obtain the most accurate absolute values.

Fig. 20 presents the subcritical rotor response spectra in the horizontal and vertical directions for the middle cross-section, and compares it with results from previous researches [3,4]. The first harmonic component is excluded from the study, since the bearing geometry has only a minor effect on it and, typically, is concerned in the balancing process of the rotor [7,9,10,12]. Moreover, the first harmonic component dominates in general the spectrum, when the rotating speed is approaching the natural frequency; the focus of the study presented here is mainly concerned on the subcritical response.

Fig. 21 reports the resonance amplitude peaks corresponding to the spectra presented in Fig. 20. The reduction of the harmonic peaks is remarkable when compared to the original geometry (highest reduction in the second harmonic for both the horizontal direction and vertical direction, −87.9% and −83.3% respectively). Compared to the cylindrical grinding and the use of adapter sleeves for the assembly, the 2nd harmonic peaks, both in the horizontal and vertical directions, and 3rd harmonic vibration component in the horizontal direction, remain

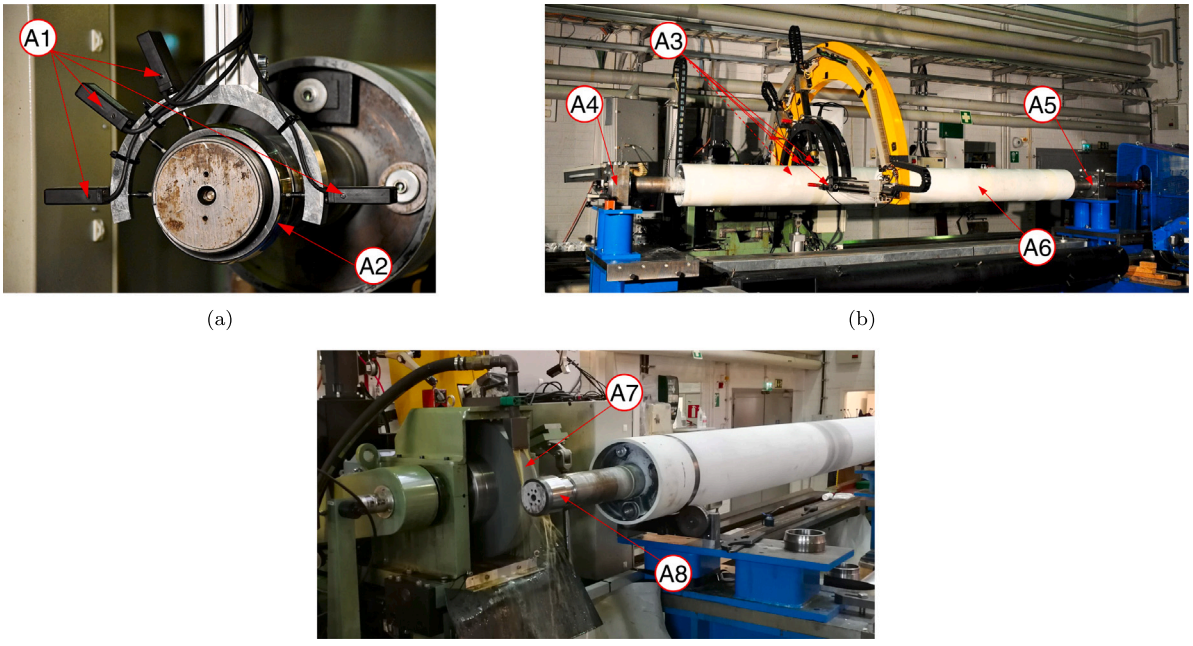

Fig. 18. (a) Measurement of the installed bearing IR roundness profiles with the four-point method [43]. (A1) Heidenhain MT 12 sensors; (A2) Bearing IR (Tending end). (b) Measurement of the rotor dynamic response with a measurement device based on the four-point method [3]. (A3) Matsushita NAIS LM 300 laser triangulation sensors; (A4) Bearing housing (Tending end); (A5) Bearing housing (Drive end); (A6) Rotor. (c) Compensative 3D grinding of the bearing installation tapered site. The tapered section was ground to the profile which minimized the roundness error of the assembled bearing IR raceways. (A7) Grinding wheel; (A8) Tapered installation seat (Tending end).

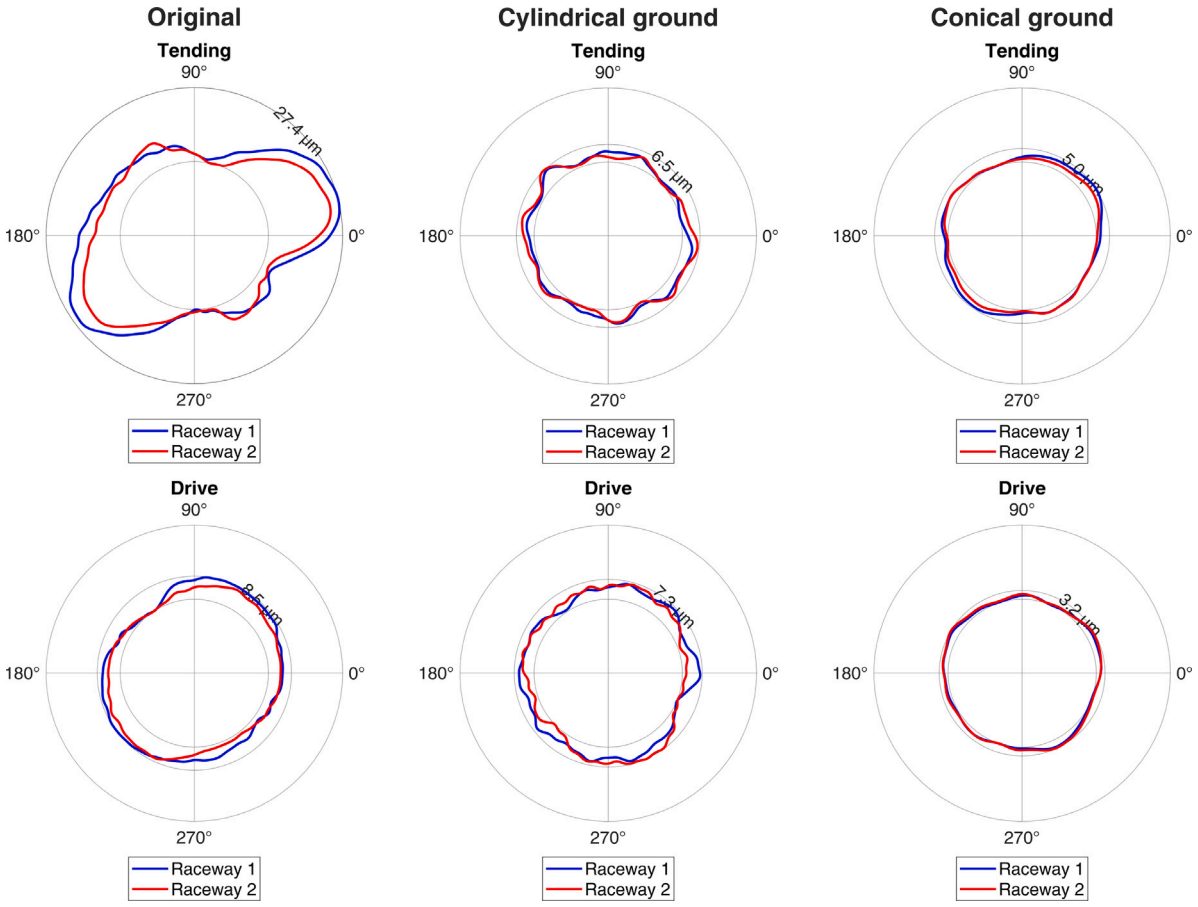

Fig. 19. Bearing IR roundness profiles for the original geometry (left), cylindrical grinding and use of an adapter sleeve (middle) [4] and conical grinding of the tapered installation seats (right). Red and blue lines represent the roundness profile measurements in the raceway mid-sections of both roller element paths.

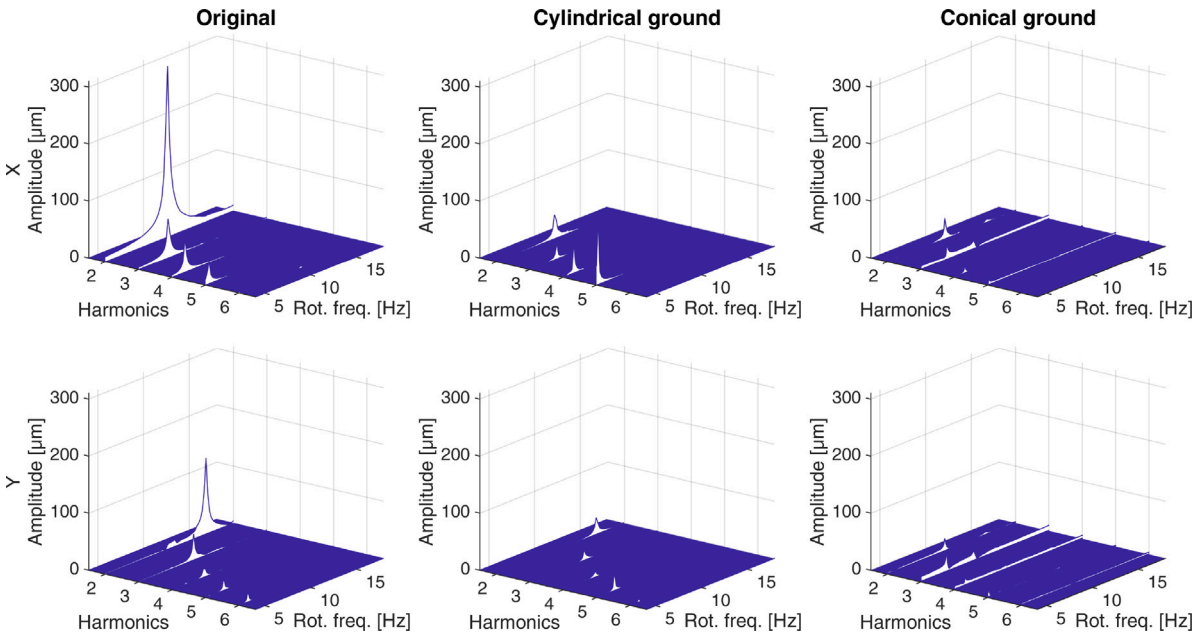

Fig. 20. Subcritical rotor response spectra in the horizontal (top row) and vertical (bottom row) directions for the middle cross-section of the original geometry (left), cylindrical grinding and use of an adapter sleeve (middle) [4] and conical grinding of the tapered installation seats (right).

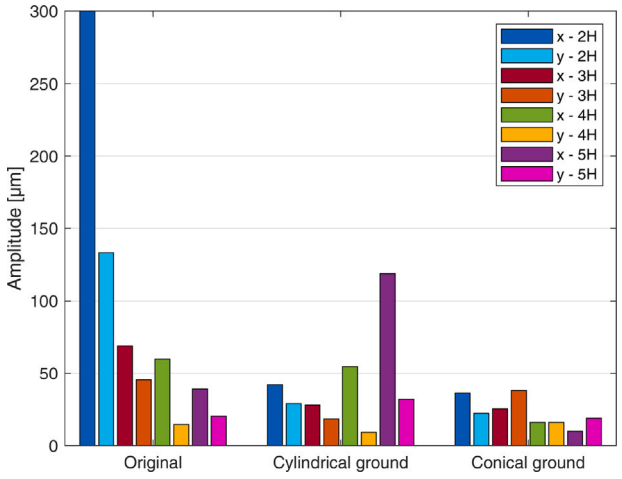

Fig. 21. Subcritical resonance peak amplitudes in the middle cross-section of the rotor in the horizontal (x) and vertical (y) directions. The amplitude values presented here correspond to the peak amplitudes of the rotor response spectra reported in Fig. 20.

almost unchanged, with a reduction of −13.9% and −23.2% for the 2nd harmonic peak in horizontal and vertical direction respectively and a reduction of −9.1% for the 3rd harmonic vibration component in the horizontal direction. The 3rd harmonic vibration component in the vertical direction increased slightly, reaching a value comparable to the same harmonic response in the horizontal direction. However, both the 4th and 5th harmonic responses decreased notably, in particular the 4th and 5th harmonic resonances in the horizontal direction, −70.1% and −91.7% respectively in the conical ground case when compared to the cylindrical one (see Table 2).

A reduction of around 10 Hz in the natural frequency in the vertical direction (in the cylindrical ground was 29.9 Hz, in the current conical ground was evaluated as 20.6 Hz) has been observed. In the horizontal direction, a negligible difference of 0.2 Hz (20.8 Hz for the cylindrical ground case, 20.6 Hz for the present conical ground one) has been noted. The differences observed in both horizontal and vertical natural frequencies of the rotor are caused by a different setting of the housing stiffnesses, that can be controlled in the experimental setup by an adjustable stiffness device [51], and were set in the current conical ground one so as to present the same natural frequency in both horizontal and vertical directions. This would not be true if the bearings were found to have non-symmetric properties along the two radial directions; in the case presented, though, the difference between the two radial directions are due to a local profile difference, with no significant effect on the natural frequency of the system.

The results clearly suggest that the compensative grinding of the conical installation seats was efficient in greatly reducing the amplitudes of all the harmonics peaks when compared to the original geometry, and allowed a reduction of the high harmonics (4th and 5th in both directions) when compared to the cylindrical case. The slight increment observed in the 3rd harmonic peak in the vertical direction is not considered notable, as the value reached in the conical ground case is in line with the 2nd and 3rd harmonic peak amplitudes of the same case under study.

The accuracy of the compensative grinding was found very satisfactory relative to the large size of the workpiece (bearing IRs residual roundness deviation lower than 5 µm, workpiece with length 5 m and external body diameter 320 mm). The 3D grinding method reported in this study does not set any upper limit to the dimensions of the workpiece. The measurement uncertainty of the four-point measurement method used in this test case was studied in previous researches and reported in [42,43,52], resulting in a sub-micrometer uncertainty in both the roundness measurements and dynamic response measurement of the rotor.

5. Conclusion

The present study successfully verified that the roundness profile of bearing IR raceways mounted on tapered shafts can be accurately evaluated though the error stacking method, i.e., the final roundness profile is equal to the sum of the shaft roundness profile plus the thickness variation of the bearing IR. The study on the effect of the relative orientation between shaft and bearing IR in the assembly process demonstrated a strong influence of the relative orientation $\Delta\alpha$ on the final roundness parameters of the raceways, with variation up to 50% of RONt, that can be exploited in the assembly process to minimize the roundness error at the locations of interest. The experimental tests

Table 2
Subcritical resonance peak amplitudes in the middle cross-section of the rotor in the horizontal and vertical directions. The amplitude values presented here correspond to the peak amplitudes of the rotor response spectra reported in Figs. 20 and 21.

Harmonics	Horizontal amplitude [μm]			Vertical amplitude [μm]		
	Original	Cylindrical ground	Conical ground	Original	Cylindrical ground	Conical ground
2	300.0	42.0	36.2	133.3	29.0	22.3
3	69.1	28.0	25.5	45.4	18.4	38.1
4	59.9	54.6	16.0	14.5	9.2	16.0
5	39.1	118.8	9.9	20.3	31.9	18.8

for different mounting conditions showed that the stacked error evaluation methodology here proposed is applicable for different mounting conditions of the components; the mounting condition did not affect the results.

These results extended the previously available literature about rolling element bearing, in which a complete study and analysis of the assembly and error stacking was missing. The successful verification of the error stacking method in evaluating the final roundness profiles of the raceways was confirmed by the Pearson's Correlation Coefficient values in the comparison between summed and experimentally measured profiles, which assumed the lowest value of 0.969, highlighting a very strong correlation between the compared profiles along the whole circumferential direction.The results obtained in the present research hold true for bearing in which the inner ring can be considered relatively thin and flexible compared to the rotor shaft, such as in large bearings. For very small bearings, for which the IR is not thin compared to the shaft, the roundness error stacking methodology may be applicable, but additional research should be conducted. Additionally, the conical taper of the rotor shaft should be manufactured within tolerance with the taper angle of the bearing inner ring, to guarantee the applicability of the roundness error stacking method.

Key outcome of the presented research is that in order to improve the roundness profile of the installed bearing IR, the thickness variation of the bearing components should be minimized. Based on the results of this research, the bearing manufacturers should concentrate on minimizing the thickness variation of the bearing IR instead of the roundness of the individual elements. The roundness of a separate IR is irrelevant, as the IR is tightened to a stiffer shaft having a roundness profile of its own. If the thickness variation of the bearing IR is minimized, the rotor manufacturer could concentrate on manufacturing the bearing installation tapered sited of the rotor with the lowest roundness deviation as possible, using for example the 3D grinding methodology here reported. An additional possibility is to measure the bearing components and the shaft installation seats in a shared angular reference system, and then assembly the components with the relative angular orientation that guarantees the lowest roundness error with the available components and their geometries. Future research may be focused on the development of simulations tools able to evaluate the stacked roundness error, allowing the development of optimization techniques of component relative orientation in order to globally minimize the final roundness of the bearing raceways.

Based on the verified stacked error methodology studied, this paper also elaborates on previous research results, extending the investigation of the total geometry of conically fitted bearings on shafts for a test case. The 3D grinding methodology was utilized to manufacture the tapered installation seats on a paper machine roll to a roundness profile, which minimized the roundness error of the installed spherical roller bearing IR raceways. The results showed that the methodology is able to reduce the roundness error of the bearing IR without grinding the ring itself, is fully functional and may next be applied to industrial processes as well. The direct installation of the bearing IR on tapered sites on the shaft successfully reduced the roundness error of both bearing IR raceways, as compared to grinding the cylindrical shaft and introducing an adapter sleeve for the assembly.

The dynamic response of the rotor was measured before and after the conical grinding operation and compared to the original dynamic measurements and the dynamic measurement after the cylindrical grinding and the use of an adapter sleeve. The results showed a significant reduction of the 4th and 5th subcritical resonance peak amplitudes when compared to the cylindrical ground case, improving the previous research results.

The methodologies here presented can be considered suitable and economic for industrial applications, especially in cases where bearing excited subcritical vibration in the rotor induce severe problems to the actual operating process. The results presented in this paper can be used to develop the design of bearing components and rotor-bearing systems.

CRediT authorship contribution statement

Lorenzo Giorio: Writing – original draft, Visualization, Software, Methodology, Investigation, Formal analysis, Data curation, Conceptualization. **Raine Viitala:** Writing – review & editing, Supervision, Methodology, Investigation, Conceptualization. **Eugenio Brusa:** Writing – review & editing, Supervision.

Declaration of competing interest

The authors declare that they have no known competing financial interests or personal relationships that could have appeared to influence the work reported in this paper.

Data availability

Data will be made available on request.

Acknowledgments

The study was founded by the 19ENG07 Met4Wind project (homepage of the project: https://www.ptb.de/empir2020/met4wind/home/), which has received funding from the EMPIR (European Metrology Research Programme) programme and from the European Union's Horizon 2020 research and innovation programme, and the acknowledgments paragraph was compiled in accordance to previously published results from the project.

References

[1] World Energy Outlook 2022, Tech. rep., International Energy Agency (IEA), 2022, p. 524, URL https://www.iea.org/reports/world-energy-outlook-2022.

[2] R. Viitala, R. Viitala, G. Gruber, B. Hemming, T. Widmaier, K. Tammi, P. Kuosmanen, Device and method for measuring thickness variation of large roller element bearing rings, Precis. Eng. 55 (2019) 59–69, http://dx.doi.org/10.1016/j.precisioneng.2018.08.007.

[3] R. Viitala, T. Widmaier, P. Kuosmanen, Subcritical vibrations of a large flexible rotor efficiently reduced by modifying the bearing inner ring roundness profile, Mech. Syst. Signal Process. 110 (2018) 42–58, http://dx.doi.org/10.1016/j.ymssp.2018.03.010.

[4] R. Viitala, Minimizing the bearing inner ring roundness error with installation shaft 3D grinding to reduce rotor subcritical response, CIRP J. Manuf. Sci. Technol. 30 (2020) 140–148, http://dx.doi.org/10.1016/j.cirpj.2020.05.002.

[5] G. Genta, C. Delprete, E. Brusa, Some considerations on the basic assumptions in rotordynamics, J. Sound Vib. 227 (3) (1999) 611–645, http://dx.doi.org/10.1006/jsvi.1999.2354.

[6] A.H. Slocum, Precision Machine Design, Prentice Hall, Englewood Cliffs, NJ, USA, 1992.

[7] Mechanical Vibration - Rotor Balancing - Part 12: Procedures and Tolerances for Rotors with Flexible Behaviour, Standard ISO 21940-12, International Organization for Standardization, 2016, p. 102, URL www.iso.org.

[8] X. Yu, General influence coefficient algorithm in balancing of rotating machinery, Int. J. Rotating Mach. 10 (2004) 85–90, http://dx.doi.org/10.1155/S1023621X04000090.

[9] H. Josephs, R. Huston, Balancing, in: Dynamics of Mechanical Systems, first ed., CRC Press, Boca Raton, FL, USA, 2002, p. 26, URL https://www.taylorfrancis.com/chapters/mono/10.1201/9781420041927-18/balancing-harold-josephs-ronald-huston.

[10] W.C. Foiles, P.E. Allaire, E.J. Gunter, Review: Rotor balancing, Shock Vib. 5 (1998) 325–336, http://dx.doi.org/10.1155/1998/648518.

[11] D.-J. Han, Generalized modal balancing for non-isotropic rotor systems, Mech. Syst. Signal Process. 21 (5) (2007) 2137–2160, http://dx.doi.org/10.1016/j.ymssp.2006.09.004.

[12] M.B. Deepthikumar, A.S. Sekhar, M.R. Srikanthan, Modal balancing of flexible rotors with bow and distributed unbalance, J. Sound Vib. 332 (24) (2013) 6216–6233, http://dx.doi.org/10.1016/j.jsv.2013.04.043.

[13] O.G. Gustafsson, T. Tallian, Study of the Vibration Characteristics of Bearings, Tech. rep., Research Laboratory SKF industries, 1963, URL https://apps.dtic.mil/sti/citations/AD0432979.

[14] E.M. Yhland, Waviness measurement-an instrument for quality control in rolling bearing industry, Proc. Inst. Mech. Eng. Conf. Proc. 182 (11) (1967) 438–445, http://dx.doi.org/10.1243/PIME_CONF_1967_182_341_02.

[15] N. Aktürk, The effect of waviness on vibrations associated with ball bearings, J. Tribol. 121 (4) (1999) 667–677, http://dx.doi.org/10.1115/1.2834121.

[16] H. Arslan, N. Aktürk, An investigation of rolling element vibrations caused by local defects, J. Tribol. 130 (4) (2008) 041101, http://dx.doi.org/10.1115/1.2958070.

[17] W. Liu, Y. Zhang, Z.-J. Feng, J.-S. Zhao, D. Wang, A study on waviness induced vibration of ball bearings based on signal coherence theory, J. Sound Vib. 333 (23) (2014) 6107–6120, http://dx.doi.org/10.1016/j.jsv.2014.06.040.

[18] J. Sopanen, A. Mikkola, Dynamic model of a deep-groove ball bearing including localized and distributed defects. Part 1: Theory, Proc. Inst. Mech. Eng. K 217 (3) (2003) 201–211, http://dx.doi.org/10.1243/14644190360713551.

[19] J. Sopanen, A. Mikkola, Dynamic model of a deep-groove ball bearing including localized and distributed defects. Part 2: Implementation and results, Proc. Inst. Mech. Eng. K 217 (3) (2003) 213–223, http://dx.doi.org/10.1243/14644190360713560.

[20] B. Ghalamchi, J.T. Sopanen, A.M. Mikkola, Dynamic model of spherical roller bearing, in: ASME 2013 International Design Engineering Technical Conferences and Computers and Information in Engineering Conference, American Society of Mechanical Engineers Digital Collection, Portland, Oregon, USA, 2013, p. 10, http://dx.doi.org/10.1115/DETC2013-12102.

[21] B. Ghalamchi, J. Sopanen, A. Mikkola, Simple and versatile dynamic model of spherical roller bearing, Int. J. Rotating Mach. 2013 (2013) e567542, http://dx.doi.org/10.1155/2013/567542.

[22] J.E. Heikkinen, B. Ghalamchi, R. Viitala, J. Sopanen, J. Juhanko, A. Mikkola, P. Kuosmanen, Vibration analysis of paper machine's asymmetric tube roll supported by spherical roller bearings, Mech. Syst. Signal Process. 104 (2018) 688–704, http://dx.doi.org/10.1016/j.ymssp.2017.11.030.

[23] E. Kurvinen, R. Viitala, T. Choudhury, J. Heikkinen, J. Sopanen, Simulation of subcritical vibrations of a large flexible rotor with varying spherical roller bearing clearance and roundness profiles, Machines 8 (2) (2020) 28, http://dx.doi.org/10.3390/machines8020028.

[24] T. Choudhury, E. Kurvinen, R. Viitala, J. Sopanen, Development and verification of frequency domain solution methods for rotor-bearing system responses caused by rolling element bearing waviness, Mech. Syst. Signal Process. 163 (2022) 108117, http://dx.doi.org/10.1016/j.ymssp.2021.108117.

[25] J. Liu, C. An, G. Pan, A vibration model of a rotor system with the sinusoidal waviness by using the non-Hertzian solution, Proc. Inst. Mech. Eng. K 236 (1) (2022) 151–167, http://dx.doi.org/10.1177/14644193211065916.

[26] J. Liu, H. Ni, R. Zhou, X. Li, Q. Xing, G. Pan, A simulation analysis of ball bearing lubrication characteristics considering the cage clearance, J. Tribol. 145 (044301) (2022) http://dx.doi.org/10.1115/1.4056358.

[27] D.G. Chetwynd, G.J. Siddall, Improving the accuracy of roundness measurement, J. Phys. E: Sci. Instrum. 9 (7) (1976) 537, http://dx.doi.org/10.1088/0022-3735/9/7/008.

[28] H. Haitjema, H. Bosse, M. Frennberg, A. Sacconi, R. Thalmann, International comparison of roundness profiles with nanometric accuracy, Metrologia 33 (1) (1996) 67, http://dx.doi.org/10.1088/0026-1394/33/1/9.

[29] M. Neugebauer, Uncertainty analysis for roundness measurements by the example of measurements on a glass hemisphere, Meas. Sci. Technol. 12 (1) (2001) 68, http://dx.doi.org/10.1088/0957-0233/12/1/309.

[30] M. Morel, H. Haitjema, Task specific uncertainty estimation for roundness measurement, in: Proc. of the 3rd Euspen International Conference, Eindhoven, The Netherlands, 2002, pp. 513–516.

[31] R. Thalmann, J. Spiller, A. Küng, O. Jusko, Calibration of Flick standards, Meas. Sci. Technol. 23 (9) (2012) 094008, http://dx.doi.org/10.1088/0957-0233/23/9/094008.

[32] H. Haitjema, Revisiting the multi-step method: Enhanced error separation and reduced amount of measurements, CIRP Ann. 64 (1) (2015) 491–494, http://dx.doi.org/10.1016/j.cirp.2015.03.001.

[33] Rolling Bearings - Tolerances - Part 1: Terms and Definitions, Standard ISO 1132-1, International Organization for Standardization, 2000, p. 76, URL www.iso.org.

[34] Y. Mao, S. Yuekang, Z. Jie-ang, Bearing thickness auto-measuring and classifying system, in: 2009 WRI World Congress on Computer Science and Information Engineering, Vol. 3, Loas Angeles, California, USA, 2009, pp. 505–509, http://dx.doi.org/10.1109/CSIE.2009.412.

[35] Y. Mao, S. Yuekang, Z. Jie-ang, MSA based on bearing thickness auto-measuring and classifying system, in: 2009 ISECS International Colloquium on Computing, Communication, Control, and Management, Vol. 3, Sanya, China, 2009, pp. 303–307, http://dx.doi.org/10.1109/CCCM.2009.5268064.

[36] S. Deng, Y. Lu, W. Zhang, X. Sun, Z. Lu, Cage slip characteristics of a cylindrical roller bearing with a trilobe-raceway, Chin. J. Aeronaut. 31 (2) (2018) 351–362, http://dx.doi.org/10.1016/j.cja.2017.07.001.

[37] Geometrical Product Specifications (GPS) - Roundness - Part 1: Vocabulary and Parameters of Roundness, Standard ISO 12181-1, International Organization for Standardization, 2011, p. 24, URL www.iso.org.

[38] D.J. Whitehouse, Handbook of Surface Metrology, Institute of Physics Publishing, Bristol, United Kingdom, 1994.

[39] Rolling Bearings - Tolerances - Part 2: Measuring and Gauging Principles and Methods, Tech. Rep. ISO 1132-1, International Organization for Standardization, 2001, URL www.iso.org.

[40] T. Widmaier, Optimisation of the Roll Geometry for Production Conditions (Doctoral Thesis), Aalto University, 2012, URL https://aaltodoc.aalto.fi:443/handle/123456789/7290.

[41] Geometrical Product Specifications (GPS) - Roundness - Part 2: Specification Operators, Standard ISO 12181-2, International Organization for Standardization, 2011, p. 24, URL www.iso.org.

[42] T. Widmaier, B. Hemming, J. Juhanko, P. Kuosmanen, V.P. Esala, A. Lassila, P. Laukkanen, J. Haikio, Application of Monte Carlo simulation for estimation of uncertainty of four-point roundness measurements of rolls, Precis. Eng. 48 (2017) 181–190, http://dx.doi.org/10.1016/j.precisioneng.2016.12.001.

[43] R. Viitala, T. Widmaier, B. Hemming, K. Tammi, P. Kuosmanen, Uncertainty analysis of phase and amplitude of harmonic components of bearing inner ring four-point roundness measurement, Precis. Eng. 54 (2018) 118–130, http://dx.doi.org/10.1016/j.precisioneng.2018.05.008.

[44] Š. Tichá, S. Adamczak, The models for the comparison of roundness profiles, J. Autom. Mob. Robot. Intell. Syst. 6 (3) (2012) 27–29, URL http://yadda.icm.edu.pl/baztech/element/bwmeta1.element.baztech-article-BUJ8-0016-0017.

[45] K. Nozdrzykowski, D. Janecki, Comparative studies of reference measurements of cylindrical surface roundness profiles of large machine components, Metrol. Meas. Syst. 11 (1) (2014) 67–76, http://dx.doi.org/10.2478/mms-2014-0007.

[46] S. Adamczak, A. Janusiewicz, W. Makieła, K. Stepień, Statistical validation of the method for measuring radius variations of components on the machine tool, Metrol. Meas. Syst. 18 (1) (2011) 35–46, http://dx.doi.org/10.2478/v10178-011-0004-5.

[47] D.J. Whitehouse, A best fit reference line for use in partial arcs, J. Phys. E: Sci. Instrum. 6 (9) (1973) 921, http://dx.doi.org/10.1088/0022-3735/6/9/034.

[48] SKF, SKF drive-up method, 2023, URL https://www.skf.com/group/products/maintenance-products/hydraulic-tools-for-mounting-and-dismounting/drive-up-method.

[49] SKF, Rolling Bearings Product Catalogue, Tech. rep., SKF, 2018, p. 1152, URL https://cdn.skfmediahub.skf.com/api/public/0901d196802809de/pdf_preview_medium/0901d196802809de_pdf_preview_medium.pdf.

[50] P. Kuosmanen, Predictive 3D Roll Grinding Method for Reducing Paper Quality Variations in Coating Machines (Doctoral Thesis), Helsinki University of Technology, Espoo, Finland, 2004, URL http://urn.fi/urn:nbn:fi:tkk-003580.

[51] R. Viitala, R. Viitala, Method and device to investigate the behavior of large rotors under continuously adjustable foundation stiffness, J. Vibroeng. 22 (5) (2020) 1037–1054, http://dx.doi.org/10.21595/jve.2020.21107.

[52] J. Juhanko, Dynamic Geometry of a Rotating Paper Machine Roll (Doctoral Thesis), Aalto University, 2011, URL https://aaltodoc.aalto.fi:443/handle/123456789/5070.